

Restore Anything Model via Efficient Degradation Adaptation

Bin Ren^{1,2,3*} Eduard Zamfir⁴ Zongwei Wu⁴ Yawei Li⁵ Yidi Li⁶
 Danda Pani Paudel³ Radu Timofte⁴ Ming-Hsuan Yang⁷ Nicu Sebe²

¹University of Pisa, ²University of Trento, ³INSAIT Sofia University, ⁴University of Würzburg,
⁵ETH Zürich, ⁶Taiyuan University of Technology, ⁷University of California, Merced

Abstract

With the proliferation of mobile devices, the need for an efficient model to restore any degraded image has become increasingly significant and impactful. Traditional approaches typically involve training dedicated models for each specific degradation, resulting in inefficiency and redundancy. More recent solutions either introduce additional modules to learn visual prompts—significantly increasing model size—or incorporate cross-modal transfer from large language models trained on vast datasets, adding complexity to the system architecture. In contrast, our approach, termed RAM, takes a unified path that leverages inherent similarities across various degradations to enable both efficient and comprehensive restoration through a joint embedding mechanism—without scaling up the model or relying on large multimodal models. Specifically, we examine the sub-latent space of each input, identifying key components and reweighting them in a gated manner. This intrinsic degradation awareness is further combined with contextualized attention in an X-shaped framework, enhancing local-global interactions. Extensive benchmarking in an all-in-one restoration setting confirms RAM’s SOTA performance, reducing model complexity by approximately 82% in trainable parameters and 85% in FLOPs. Our code and models will be publicly available.

1. Introduction

Image restoration (IR) is a fundamental task within low-level computer vision, aiming to enhance the quality of images affected by numerous factors, including noise [89–91], blur [31, 52, 64, 67], compression artifacts [16, 21, 28], adverse weather conditions [2, 3, 36–38, 77], and other forms of distortion. It supports downstream vision tasks such as object detection, recognition, and tracking [4, 45, 50, 56, 63]. Despite significant advances in recent years, existing IR methods struggle to efficiently handle complex distortions while preserving or recovering essential image de-

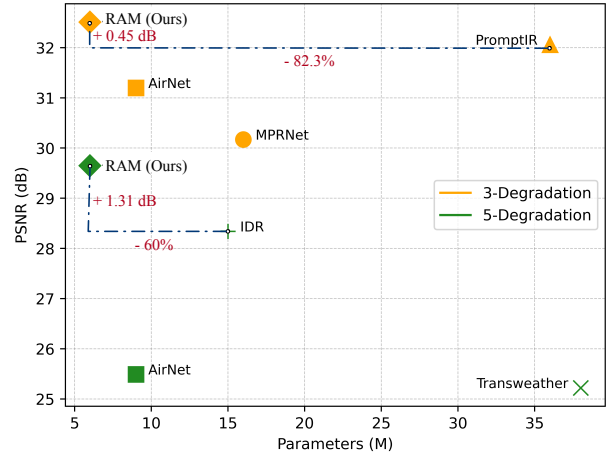


Figure 1. Average PSNR and parameters comparison (*i.e.*, our RAM archives 0.45 dB PSNR improvement with around 82% parameters reduced compared to the SOTA PromptIR [53])

tails [39, 56]. The state-of-the-art methods often impose a substantial computational burden, limiting their applicability, especially on edge and mobile devices. Thus, there is a strong demand for an efficient model to handle any type of image degradation.

The complexity of existing restoration models [5, 42, 73, 84, 86] arises mainly from the diversity of the types of degradation. Consequently, many existing methods are tailored for a specific type of degradation and application with limited generalization to others. A versatile system would require the integration of multiple specialized models, resulting in a complex and heavy framework. Some recent work has shown that a single architecture can address multiple types of degradation, but these approaches lack parameter unification, leading to multiple checkpoints, each for a specific task [5, 8, 73, 86]. Although this reduces system complexity, it compromises efficiency due to the increased number of checkpoint sets.

Recent studies have focused on achieving both architectural and parameter unification [34, 46, 53, 82, 88]. Diffusion-based methods have demonstrated improved im-

*Work done during visiting at INSAIT Sofia University.

age generation capabilities [30, 58, 95]. To improve the controllability of the network, other approaches treat each modality as an independent visual prompt, which guides the network toward the target application [41, 53, 70]. Another group of works uses text as an intermediate representation to unify all degradations, using textual instructions to prompt the network [12, 49]. Despite promising results, these networks still require significant computational resources, with a huge number of parameters and low inference speed.

In this paper, we propose a novel perspective that treats image restoration as a unified problem, arguing that *despite degradation-specific characteristics, all restoration tasks share underlying similarities*. Since all types of restoration require an understanding of the global context to preserve structural integrity, while also being sensitive to local details and capable of reducing noise affecting quality. Learning these general techniques is not limited to one specific task, but is generalizable and applicable across various types of degradation. This aligns with the motivation behind recent advancements in large language models (LLMs), which have demonstrated the potential to learn a joint embedding or utilize a single network for multiple tasks. Unlike LLMs that achieve unified parameters through learning from large data priors with substantial models, we focus on deeply extracting the inherent details of a single image to build correlations across degradations. Our approach enables us to achieve comparable performance without the need for specific modules and unique parameter sets, resulting in significantly fewer parameters and enabling emergent alignment in image restoration.

To efficiently achieve such a unification, we propose a novel lightweight attention mechanism that optimally intertwines global context and local details. Specifically, we introduce a gated local block that learns degradation-aware details, aiming to discern different degradation types and handle nuanced differences at a detailed level. Technically, for each feature, we analyze its detailed components, comprising the ego, shifted, and scaled parts. Leveraging the network’s self-adaptation capability, we reweight and gate the contribution of each key component intelligently and adaptively, reshaping the output into a locally optimized form with enhanced awareness of its degradation type. This local awareness is then integrated with transformer attention in an X-shaped scheme to maximize the local-global intertwining. Note that for feature modeling, we split the input feature into subparts and process them in a sub-latent space before final aggregation. This strategy not only enables inner-feature interaction but also reduces computational cost, making our model both effective and efficient.

The contributions of this work are:

- We propose RAM, a single model capable of efficiently handling any type of degradation. Compared to the SOTA all-in-one counterparts, our model reduces the compu-

tational cost by 85.6% while delivering superior overall performance.

- We introduce a novel local-global gated intertwining within the feature modeling block. This design deeply explores the intrinsic characteristics of each degradation type as guidance, without the need for a degradation-specific design, leading to a cohesive embedding for comprehensive IR.
- Extensive comparisons across different IR tasks validate the effectiveness and efficiency of our proposed method. We hope our efficient network can serve as a baseline and inspire future research in the domain.

2. Related Work

Image Restoration (IR). Image restoration aims to solve a highly ill-posed problem by reconstructing high-quality images from their degraded counterparts. Due to its importance, IR has been applied to various applications [1, 40, 61, 83]. Initially, IR was addressed through model-based solutions involving the search for solutions to specific formulations. However, learning-based approaches have gained much attention with the significant advancements in deep neural networks. Numerous approaches have been developed, including regression-based [7, 32, 39, 42, 43, 92] and generative model-based pipelines [24, 44, 48, 72, 81, 95] that built on convolutional [16, 71, 89, 90], MLP [68], state space mode [15, 25, 26, 96], or vision transformers-based (ViTs) architectures [18, 39, 42, 55, 86]. Although state-of-the-art methods have achieved promising performance, the mainstream IR solutions still focus on addressing single degradation tasks such as denoising [90, 94], dehazing [60, 76], deraining [29, 57], deblurring [31, 58], and so on. In this work, the proposed method is built based on the regression-based pipeline with ViT architecture.

One for Any Image Restoration. Training a task-specific model to tackle a single type of degradation is effective, but practical implementation is challenging due to the need for separate models for each degradation type. In reality, images often suffer from multiple degradations and artifacts, making it difficult to address them individually. Task-specific solutions require significant computing and storage resources, substantially increasing their environmental impact. To address this, the emerging All-in-One image restoration field uses a single-blind restoration model to handle multiple degradation types simultaneously. Specifically, AirNet [35] accomplishes blind All-in-One image restoration by leveraging contrastive learning to derive degradation representations from corrupted images, which are then used to reconstruct the clean image. Following this, IDR [88] addresses All-in-One image restoration by decomposing image degradations into their fundamental physical principles and employing a two-stage meta-learning approach. More recently, the

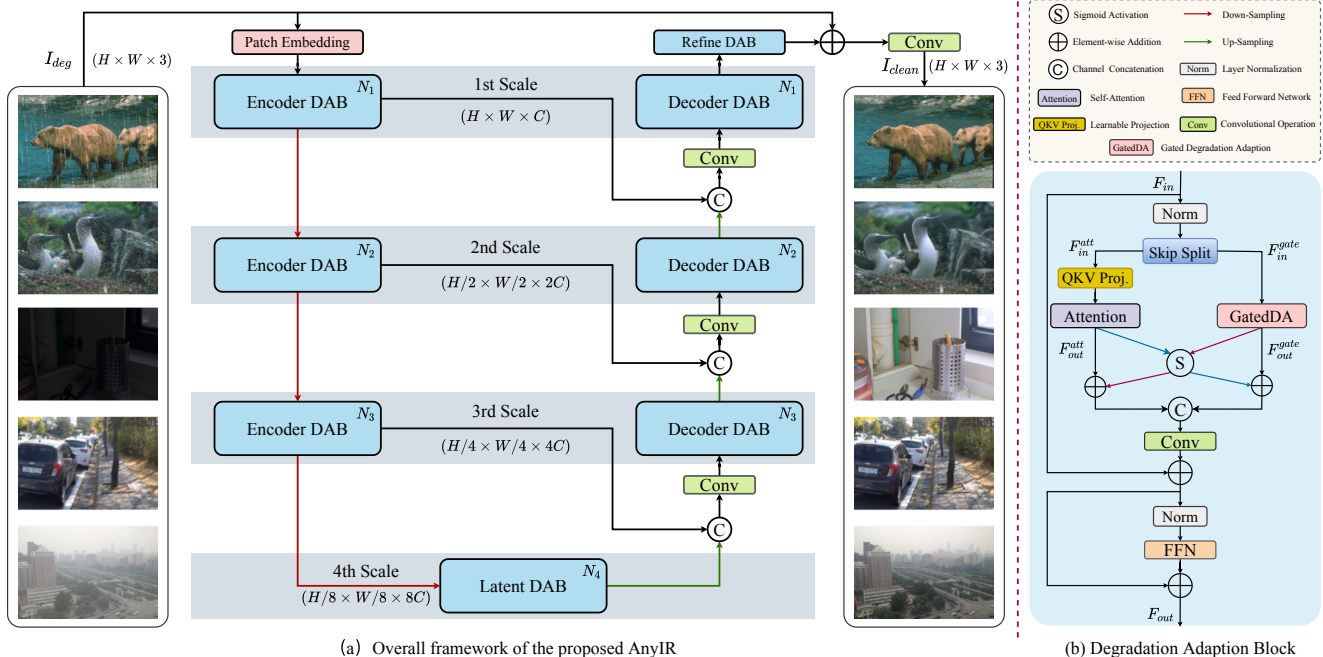


Figure 2. (a) Overall framework of the proposed RAM : a U-shaped structure which mainly consists of a convolutional patch embedding, a U-shape encoder-decoder main body, and an extra refined block. (b) Structure of each degradation adaptation block (DAB)

prompt-based paradigm [41, 53, 70] has been introduced, incorporating an additional visual prompt learning module. This approach has been validated as effective in guiding a single trained model to better restore images with multiple types of degradation by leveraging the learned discriminative capabilities of the visual prompts. Built upon the prompt-based paradigm, there also some recent works propose modeling the visual prompt either from the frequency perspective [13] or by posting more complex architecture designs with extra dataset [20, 82]. However, using visual prompt modules often leads to longer training times and reduced efficiency. Instead, our work enhances the model’s ability to capture representative information without the burden of heavy and complex prompt modules.

3. Proposed RAM

Overview. In this section, we present our efficient All-in-One restoration method, termed RAM . The overall framework is illustrated in Fig. 2. At a macro level, RAM employs a U-shaped network architecture [62] with four levels. Each level incorporates $N_i, i \in [1, 2, 3, 4]$ instances of our novel Degradation Adaptation Blocks (DAB) 3.1, and each DAB is built upon the proposed gated degradation adaption (GatedDA) module (Sec. 3.2). Initially, a convolutional layer first extracts shallow features from the degraded input, creating a patch embedding of $H \times W \times C$. Subsequently, each U-Net level doubles the embedding dimension and halves the spatial resolution. Skip connections transfer information from the encoder stage to the decoder. At the decoder, we

merge these features with the signal from the previous decoding stage using a linear projection. Lastly, a global residual connection links the input image to the output, preserving high-frequency details and producing the restored image.

3.1. Degradation Adaptation Block

Our objective is to minimize the overall computational complexity while proficiently encapsulating the spatial data crucial for image restoration. Neural meta-architectures have gained significant attention in computer vision [47, 79, 80], with convolutional-based networks achieving performance comparable to Transformers. Recently, Mamba-based models [15, 25, 26] have revisited the concept of gated blocks, simplifying the meta-architecture into an integration of a spatial mixer convolution and a Feed-forward network. For achieving an efficient image restorer, we propose a hybrid architecture, combining a parameter-reduced Attention layer for global feature learning, while a gated convolutional block aggregates degradation-specific local details.

The detailed structure of the proposed DAB is illustrated in Fig. 2 (b). Given an input feature tensor $F_{in} \in \mathbb{R}^{H \times W \times C}$, where H, W , and C denote the height, width, and channel dimensions, respectively, we employ a selective channel-wise partitioning strategy defined as follows:

$$\begin{aligned}
 F_{in}^{att} &= \{F_{in}^{(2k-1)} \mid k \in \mathbb{Z}^+, k \leq \frac{C}{2}\}, \\
 F_{in}^{gate} &= \{F_{in}^{(2k)} \mid k \in \mathbb{Z}^+, k \leq \frac{C}{2}\},
 \end{aligned} \tag{1}$$

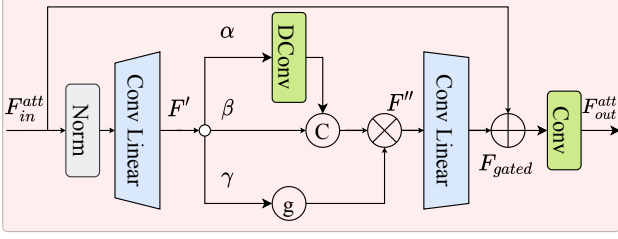


Figure 3. Structure of our GatedDA. \oplus , \odot , \otimes , and \otimes denote the element-wise addition, channel-wise concatenation, GELU [27] activation, and element-wise multiplication, respectively.

where F_{in}^{att} and $F_{in}^{gate} \in \mathbb{R}^{H \times W \times C/2}$ denote the sub-features derived from interleaved sampling along the channel dimension. This setup provides two distinct pathways: F_{in}^{att} , focusing on attention modulation, and F_{in}^{gate} , specializing in gated transformation. This structured skip-split offers two notable benefits, *i.e.*, (i) Significant Complexity Reduction: By reducing the effective channel dimension in each pathway, the overall model complexity and parameter count are notably minimized, which is particularly beneficial for the self-attention layers in Vision Transformers (ViTs) [18]. (ii) Improved Information Retention: Unlike conventional half-split methods, the skip-split preserves feature diversity by uniformly sampling the original channels, ensuring each subset retains comprehensive information from F_{in} without loss of essential channel-wise details.

To capture the complex dependencies inherent to global degradation, we employ a multi-depth convolution head attention mechanism [53, 86] on the feature subset F_{in}^{att} , resulting in F_{out}^{att} . This attention approach is particularly effective for image restoration, where degradation is often non-uniform and shaped by various intricate factors. Specifically, F_{in}^{att} is transformed into Query (Q), Key (K), and Value (V) matrices, defined as: $Q = F_{in}^{att} \mathbf{W}_{qry}$, $K = F_{in}^{att} \mathbf{W}_{key}$, $V = F_{in}^{att} \mathbf{W}_{val}$, where \mathbf{W}_{qry} , \mathbf{W}_{key} , and \mathbf{W}_{val} are learnable weights. The output F_{out}^{att} is then calculated as:

$$F_{out}^{att} = \sum_i \text{Softmax} \left(\frac{QK^T}{\sqrt{d}} \right)_i V_{i,j}, \quad (2)$$

where \sqrt{d} is a scaling factor to normalize attention scores, stabilizing gradients and aiding convergence. This attention mechanism excels at modeling long-range dependencies across the feature space, a vital capability for image restoration where degradation—such as noise, blur, and artifacts—exhibits spatial correlations yet varies across the image [6, 39, 42, 86]. By leveraging this global modeling, the framework dynamically identifies and emphasizes degraded regions, preserving fine details essential for high-quality restoration.

Meanwhile, the proposed GatedDA operation (see

Algorithm 1 Gated Degradation Adaption

Require: Input $F_{in}^{gate} \in \mathbb{R}^{C \times H \times W}$, initial temperature τ
Ensure: Output $F_{out}^{gate} \in \mathbb{R}^{C \times H \times W}$

- 1: $\hat{F} \leftarrow \text{Norm}(F_{in}^{gate})$ // Normalize
- 2: $\mu, \sigma \leftarrow \frac{1}{HW} \sum \hat{F}, \sqrt{\frac{1}{HW} \sum (\hat{F} - \mu)^2}$ // Mean, std
- 3: $\alpha \leftarrow \sigma(\mu + \sigma)$ // Temp adjust
- 4: $\tau_{adj} \leftarrow \tau \cdot \alpha$
- 5: $F' \leftarrow \hat{F} \mathbf{W}_{exp}$ // Channel expand
- 6: $\gamma, \beta, \alpha \leftarrow \text{split}(F')$ // Split γ, β, α
- 7: $\alpha' \leftarrow (\alpha \mathbf{W}_{depth}) \cdot \tau_{adj}$ // Depthwise conv
- 8: $F_{gated} \leftarrow \sigma(\gamma) \cdot \text{concat}(\beta, \alpha') \mathbf{W}_{gate}$ // Gate combine
- 9: $F_{out}^{gate} \leftarrow (F_{gated} + F_{in}^{gate}) \mathbf{W}_{proj}$ // Residual, proj
- 10: **return** F_{out}^{gate}

Sec. 3.2) is applied to F_{in}^{gate} , producing F_{out}^{gate} . This approach combines the strengths of attention and convolution: the attention module captures global structural cues essential for overall image context, while the convolutional pathway captures local dependencies crucial for refining details in low-level vision tasks [9, 10, 42]. To enable effective interaction between these global and local features, we introduce a cross-feature update:

$$\begin{aligned} F_{out}^{ag} &= F_{out}^{att} + \sigma(F_{out}^{gate}), \\ F_{out}^{ga} &= F_{out}^{gate} + \sigma(F_{out}^{att}), \end{aligned} \quad (3)$$

where $\sigma(\cdot)$ is the Sigmoid activation, enhancing each feature map with complementary information. Through this update, F_{out}^{att} gains local detail sensitivity, while F_{out}^{gate} benefits from structural context. The fused representation F_{fuse} is then computed by concatenating F_{out}^{att} and F_{out}^{gate} , followed by a convolution with learnable weights \mathbf{W}_{fuse} and a residual connection to the input:

$$F_{fuse} = \text{Conv} \mathbf{W}_{fuse} (\text{concat}(F_{out}^{att}, F_{out}^{gate})) + F_{in}. \quad (4)$$

This fusion step integrates global and local information, enhancing feature richness for the final restoration. Next, layer normalization, a feed-forward network (FFN), and a residual connection are applied, yielding F_{out} :

$$F_{out} = \text{FFN}(\text{Norm}(F_{fuse})) + F_{fuse}. \quad (5)$$

This sequence stabilizes feature distributions and boosts expressive capacity, effectively combining global and local cues for high-fidelity, detailed image restoration.

3.2. Gated Degradation Adaption

To capture local degradation-aware details, we leverage the selective properties of gated convolution. Given an input feature map $F_{in}^{gate} \in \mathbb{R}^{C \times H \times W}$, a layer normalization is first applied to stabilize feature distributions, followed by

Table 1. Comparison to state-of-the-art on three degradations. PSNR (dB, \uparrow) and SSIM (\uparrow) metrics are reported on the full RGB images. **Best** and **second best** performances are highlighted. Our method sets a new state-of-the-art on average across all benchmarks while being significantly more efficient than prior work. ‘-’ represents unreported results.

| Method | Params. | Dehazing | | Deraining | | Denoising | | | Average | | | | |
|--|-----------|--------------|-------------|----------------------|----------------------|----------------------|-------------|--------------|-------------|--------------|-------------|--------------|-------------|
| | | SOTS | Rain100L | BSD68 $_{\sigma=15}$ | BSD68 $_{\sigma=25}$ | BSD68 $_{\sigma=50}$ | | | | | | | |
| BRDNet [65] | - | 23.23 | .895 | 27.42 | .895 | 32.26 | .898 | 29.76 | .836 | 26.34 | .693 | 27.80 | .843 |
| LPNet [23] | - | 20.84 | .828 | 24.88 | .784 | 26.47 | .778 | 24.77 | .748 | 21.26 | .552 | 23.64 | .738 |
| FDGAN [17] | - | 24.71 | .929 | 29.89 | .933 | 30.25 | .910 | 28.81 | .868 | 26.43 | .776 | 28.02 | .883 |
| DL [22] | 2M | 26.92 | .931 | 32.62 | .931 | 33.05 | .914 | 30.41 | .861 | 26.90 | .740 | 29.98 | .876 |
| MPRNet [85] | 16M | 25.28 | .955 | 33.57 | .954 | 33.54 | .927 | 30.89 | .880 | 27.56 | .779 | 30.17 | .899 |
| AirNet [34] | 9M | 27.94 | .962 | 34.90 | .967 | 33.92 | .933 | 31.26 | .888 | 28.00 | .797 | 31.20 | .910 |
| PromptIR [53] | 36M | 30.58 | .974 | 36.37 | .972 | 33.98 | .933 | 31.31 | .888 | 28.06 | .799 | 32.06 | .913 |
| RAM (Ours) | 6M | 31.38 | .979 | 37.90 | .981 | 33.95 | .933 | 31.30 | .889 | 28.04 | .797 | 32.51 | .916 |
| Methods with the assistance of vision language, multi-task learning, natural language prompts, and multi-modal control | | | | | | | | | | | | | |
| DA-CLIP [49] | 125M | 29.46 | .963 | 36.28 | .968 | 30.02 | .821 | 24.86 | .585 | 22.29 | .476 | - | - |
| Art _{PromptIR} [75] | 36M | 30.83 | .979 | 37.94 | .982 | 34.06 | .934 | 31.42 | .891 | 28.14 | .801 | 32.49 | .917 |
| InstructIR-3D [11] | 16M | 30.22 | .959 | 37.98 | .978 | 34.15 | .933 | 31.52 | .890 | 28.30 | .804 | 32.43 | .913 |
| UniProcessor [19] | - | 31.66 | .979 | 38.17 | .982 | 34.08 | .935 | 31.42 | .891 | 28.17 | .803 | 32.70 | .918 |

a 1×1 convolution that expands the channel dimension to $\text{hidden} = r_{\text{expan}} \cdot C$, where r_{expan} is the expansion ratio, as shown in Alg. 1. To adaptively respond to varying intensities, we introduce a temperature adjustment mechanism. Based on the input’s mean and standard deviation, the initial temperature τ is modulated as $\tau_{\text{adj}} = \tau \cdot \alpha$, where α serves as a dynamic scaling factor (see steps 2–4 of Algorithm 1). This temperature adjustment enhances the model’s sensitivity to subtle degradation patterns, promoting detailed feature capture. The expanded feature F' is then split into three parts: γ , β , and α (as shown in step 6). Here, α undergoes depthwise convolution with τ_{adj} to capture spatial details, β retains the original information, and γ is activated with GELU [27] to enable a non-linear gated selection mechanism. These components are recombined and modulated, selectively emphasizing critical features (step 7). Finally, F'' is projected back to the original channel dimension and combined with $F_{\text{in}}^{\text{gate}}$ through a skip connection to prevent information loss. A final 1×1 convolution fuses the degradation-adapted features with the input, yielding the output $F_{\text{out}}^{\text{gate}}$ (steps 8–9 in Algorithm 1). In summary, the GatedDA block dynamically adjusts temperature and gating mechanisms to adaptively capture degradation-sensitive features, balancing global structure with fine detail. Further analysis is available in the *Supplementary Materials* (i.e., *Supp. Mat.*).

4. Experiments and Comparisons

We conduct experiments adhering to the protocols of prior general image restoration works [53, 88] under two settings: (i) *All-in-One* and (ii) *Single-task*. In the *All-in-One* setting, a unified model is trained to handle multiple degradation types, considering *three* and *five* distinct degradations. In the *Single-task* setting, separate models are trained for each specific restoration task. The implementation details and the

dataset introduction are provided in our *Supp. Mat.*

4.1. State of the Art Comparison

Three Degradations. We evaluate our All-in-One restorer, RAM, against other specialized methods, including BRDNet [66], LPNet [23], FDGAN [17], DL [22], MPRNet [85], AirNet [34], and PromptIR [53], all trained on three degradations: dehazing, deraining, and denoising. RAM consistently leads as the top-performing All-in-One restorer, with an average gain of 0.45 dB across benchmarks and the most efficient architecture, as shown in Tab. 1. It achieves state-of-the-art results on SOTS and Rain100L, outperforming PromptIR by 0.38 dB and 1.83 dB, respectively. In denoising, RAM ranks second across all σ levels while maintaining 80% fewer parameters and FLOPs.

Five Degradations. Extending the three degradation tasks to include deblurring and low-light enhancement [34, 88], we validate our method’s comprehensive performance in an All-in-One setting. As shown in Tab. 2, RAM effectively leverages degradation-specific features, surpassing AirNet [34] and IDR [88] by an average of 4.16 dB and 1.22 dB, respectively, with 33% and 60% fewer parameters. Against general image restorers, RAM outperforms Restormer [86] and NAFNet [5] on the LOLv1 dataset by 3.09 dB and 3.01 dB, while being four times smaller than Restormer and three times smaller than NAFNet.

Single-Degradation. We present results in Tab. 3 with RAM trained on individual degradation tasks: dehazing, deraining, and denoising. For dehazing, RAM achieves the second-best PSNR and the highest SSIM. In deraining, RAM surpasses the previous state-of-the-art, PromptIR [53], by 0.75 dB in PSNR and 0.003 in SSIM. For denoising, RAM ranks second overall, effectively reducing noise while preserving details. Notably, while other models show significant performance

Table 2. Comparison to state-of-the-art on five degradations. PSNR (dB, \uparrow) and SSIM (\uparrow) metrics are reported on the full RGB images with (*) denoting general image restorers, others are specialized all-in-one approaches. **Best** and **second best** performances are highlighted.

| Method | Params. | Dehazing | | Deraining | | Denoising | | Deblurring | | Low-Light | | Average |
|--|-----------|--------------|-------------|--------------|-------------|----------------------|-------------|--------------|-------------|--------------|-------------|--------------------------|
| | | SOTS | | Rain100L | | BSD68 $_{\sigma=25}$ | | GoPro | | LOLv1 | | |
| NAFNet* [5] | 17M | 25.23 | .939 | 35.56 | .967 | 31.02 | .883 | 26.53 | .808 | 20.49 | .809 | 27.76 .881 |
| DGUNet* [51] | 17M | 24.78 | .940 | 36.62 | .971 | 31.10 | .883 | 27.25 | .837 | 21.87 | .823 | 28.32 .891 |
| SwinIR* [42] | 1M | 21.50 | .891 | 30.78 | .923 | 30.59 | .868 | 24.52 | .773 | 17.81 | .723 | 25.04 .835 |
| Restormer* [86] | 26M | 24.09 | .927 | 34.81 | .962 | 31.49 | .884 | 27.22 | .829 | 20.41 | .806 | 27.60 .881 |
| MambaIR* [26] | 27M | 25.81 | .944 | 36.55 | .971 | 31.41 | .884 | 28.61 | .875 | 22.49 | .832 | 28.97 .901 |
| DL [22] | 2M | 20.54 | .826 | 21.96 | .762 | 23.09 | .745 | 19.86 | .672 | 19.83 | .712 | 21.05 .743 |
| Transweather [69] | 38M | 21.32 | .885 | 29.43 | .905 | 29.00 | .841 | 25.12 | .757 | 21.21 | .792 | 25.22 .836 |
| TAPE [46] | 1M | 22.16 | .861 | 29.67 | .904 | 30.18 | .855 | 24.47 | .763 | 18.97 | .621 | 25.09 .801 |
| AirNet [34] | 9M | 21.04 | .884 | 32.98 | .951 | 30.91 | .882 | 24.35 | .781 | 18.18 | .735 | 25.49 .847 |
| IDR [88] | 15M | 25.24 | .943 | 35.63 | .965 | 31.60 | .887 | 27.87 | .846 | 21.34 | .826 | 28.34 .893 |
| PromptIR [53] | 36M | 26.54 | .949 | 36.37 | .970 | 31.47 | .886 | 28.71 | .881 | 22.68 | .832 | 29.15 .904 |
| RAM (ours) | 6M | 29.84 | .977 | 36.91 | .977 | 31.15 | .882 | 26.86 | .822 | 23.50 | .845 | 29.65 .901 |
| Methods with the assistance of natural language prompts and large vision model | | | | | | | | | | | | |
| InstructIR [11] | 16M | 36.84 | .973 | 27.10 | .956 | 31.40 | .887 | 29.40 | .886 | 23.00 | .836 | 29.55 .907 |
| Perceive-IR [93] | 42M | 28.19 | .964 | 37.25 | .977 | 31.44 | .887 | 29.46 | .886 | 22.88 | .833 | 29.84 .909 |

Table 3. Comparison to state-of-the-art for single degradations. PSNR (dB, \uparrow) and SSIM (\uparrow) metrics are reported on the full RGB images. **Best** and **second best** performances are highlighted. Our method excels prior work on dehazing and deraining.

| (a) Dehazing | | | (b) Deraining | | | (c) Denoising | | | | |
|---------------|-----------|--------------------------|---------------|-----------|--------------------------|---------------|-----------|--------------------------|--------------------------|--------------------------|
| Method | Params. | SOTS | Method | Params. | Rain100L | Method | Params. | $\sigma=15$ | $\sigma=25$ | $\sigma=50$ |
| DehazeNet [3] | - | 22.46 .851 | DIDMDN [87] | - | 23.79 .773 | CBM3D [14] | - | 33.50 .922 | 30.69 .868 | 27.36 .763 |
| MSCNN [59] | - | 22.06 .908 | UMR [78] | - | 32.39 .921 | DnCNN [89] | - | 33.89 .930 | 31.23 .883 | 27.92 .789 |
| AODNet [33] | - | 20.29 .877 | SIRR [74] | - | 32.37 .926 | IRCNN [90] | - | 33.87 .929 | 31.18 .882 | 27.88 .790 |
| EPDN [54] | - | 22.57 .863 | MSPFN [29] | - | 33.50 .948 | FFDNet [91] | - | 33.87 .929 | 31.21 .882 | 27.96 .789 |
| FDGAN [17] | - | 23.15 .921 | LPNet [23] | - | 23.15 .921 | BRDNet [65] | - | 34.10 .929 | 31.43 .885 | 28.16 .794 |
| AirNet [34] | 9M | 23.18 .900 | AirNet [34] | 9M | 34.90 .977 | AirNet [34] | 9M | 34.14 .936 | 31.48 .893 | 28.23 .806 |
| PromptIR [53] | 36M | 31.31 .973 | PromptIR [53] | 36M | 37.04 .979 | PromptIR [53] | 36M | 34.34 .938 | 31.71 .897 | 28.49 .813 |
| RAM (ours) | 6M | 30.92 .979 | RAM (ours) | 6M | 37.79 .982 | RAM (ours) | 6M | 34.27 .937 | 31.63 .896 | 28.39 .810 |

drops in multi-degradation settings, RAM maintains robust performance, attributed to its unified cross-degradation embedding. Furthermore, RAM is substantially smaller than competing models, highlighting its efficiency and practical feasibility.

Visual results. To complement the quantitative results, we visualize the outcomes of our method in Fig. 4. The visualizations demonstrate the efficacy of RAM across dehazing and draining, and we marked out the detailed region via the red boxes. The denoising visual results are provided in our *Supp. Mat.* In the dehazing task, both AirNet [34] and PromptIR [53] exhibit limitations in fully eliminating haziness, leading to noticeable color reconstruction discrepancies. In contrast, our RAM method effectively enhances visibility and ensures precise color reconstruction. In challenging rainy scenes, previous methods continue to exhibit remnants of rain streaks. Please, **zoom in** for more details. In contrast, our approach excels at eliminating these artifacts and recovering underlying details, showing our superiority under adverse weather conditions. Note that the current SOTA PromptIR is approximately $6\times$ larger than ours. De-

Table 4. Complexity Analysis. FLOPs are computed on an input image of size 224×224 using a NVIDIA Tesla A100 (40G) GPU.

| Method | PSNR (dB, \uparrow) | Memory (\downarrow) | Params. (\downarrow) | FLOPs (\downarrow) |
|---------------|------------------------|-------------------------|--------------------------|------------------------|
| AirNet [34] | 31.20 | 4829M | 8.93M | 238G |
| PromptIR [53] | 32.06 | 9830M | 35.59M | 132G |
| IDR [88] | - | 4905M | 15.34M | 98G |
| RAM (ours) | 32.51 | 3556M | 6.29M | 19G |

spite this, our method consistently produces visually superior results, demonstrating its effectiveness. For more detailed examples, please refer to the *Supp. Mat.*

Model efficiency. Tab. 4 compares memory usage, FLOPs, and model parameters, highlighting our framework’s efficiency over state-of-the-art all-in-one restorers. With a hybrid block design and our proposed degradation adaptation module, RAM achieves a 0.45 dB PSNR improvement over PromptIR [53] while using 63.8% less memory, 82.3% fewer parameters, and only 19G FLOPs, making it **85.6%** more computationally efficient. This efficiency is due to our global-local intertwining in the sub-latent space, enabling both high performance and practical applicability. Our significant reductions in memory, parameters, and FLOPs position

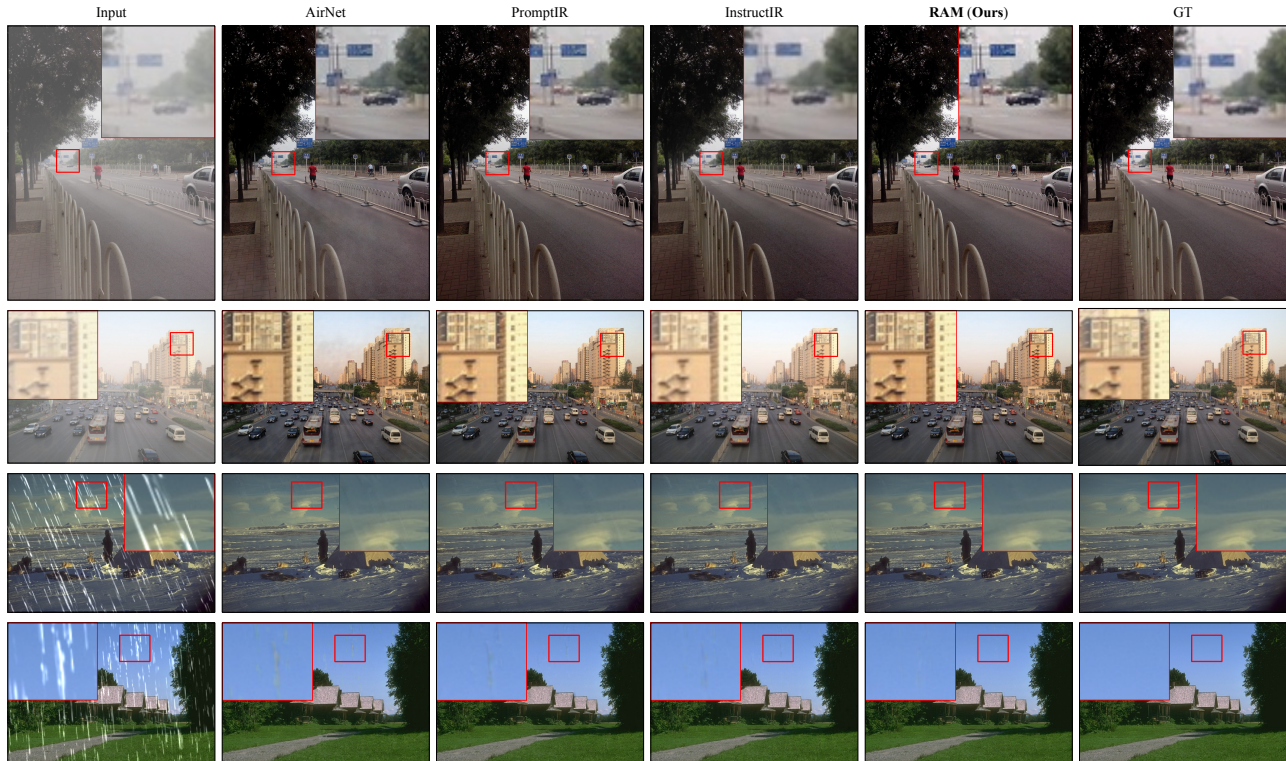


Figure 4. Visual comparison of RAM with state-of-the-art methods considering three degradations. Zoom in for a better view.

Table 5. Ablation comparison of the effect of each component under the 3-degradation all-in-one task. The average PSNR is reported.

| Method | Skip-Split | Cross-Sigmod | GatedDA | PSNR (dB, \uparrow) |
|--------|------------|--------------|---------|------------------------|
| (a) | × | × | × | 30.85 |
| (b) | ✓ | × | × | 31.83 |
| (c) | × | × | ✓ | 32.13 |
| (d) | ✓ | × | ✓ | 32.35 |
| (e) | ✓ | ✓ | ✓ | 32.51 |

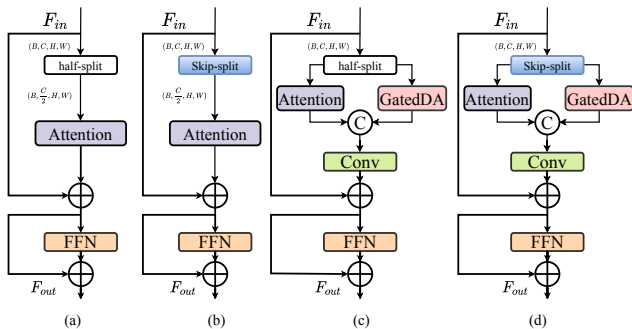


Figure 5. Structure of different DAB variants.

RAM as a strong, efficient baseline for future research.

4.2. Ablation Studies

Impact of different components. We conduct detailed studies on the proposed components within our RAM framework. All experiments are conducted in the *All-in-One* setting with

Table 6. Results of different (α, β, γ) for three-degradation.

| (α, β, γ) | PSNR (dB, \uparrow) | SSIM (\downarrow) |
|--------------------------------|------------------------|-----------------------|
| (0, hidden/2, hidden/2) | 32.14 | .910 |
| (hidden/2, 0, hidden/2) | 32.21 | .912 |
| (hidden/2, hidden/2, 0) | 31.37 | .907 |
| (hidden/4, hidden/4, hidden/2) | 32.51 | .916 |

three degradations. We compare our plain feature modeling block DAB against other variants. As detailed in Tab. 5, we assess the effectiveness of our key architectural contributions by removing or replacing our designed module with the counterparts. The detailed architecture overview of these considered counterparts can be found in Fig. 5.

We first examine the impact of our skip-split operation (a-b), which yields a significant improvement of 1.02 dB over the common half-split method. This validates and supports our motivation of deeply enabling the intertwining within the subparts of an input feature. Introducing our proposed GatedDA in parallel to the attention layer (c) results in a substantial increase of 1.27 dB. Combining GatedDA with the skip-split operation (d) further enhances the reconstruction fidelity of our framework. This validates the effectiveness of our intention of using the local gated details to reconstruct the degradation-aware output. Lastly, the introduction of cross-feature filtering (e), please refer to Fig. 2 for our plain design, improves the interconnectivity between global-local features, further benefiting overall performance.



Figure 6. Visual feature maps of α , β , and γ within GatedDA.

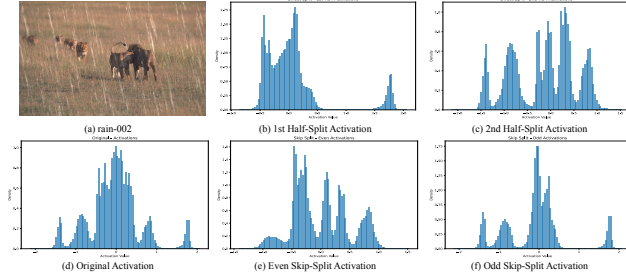


Figure 7. Visualization of the channel activation distribution.

Impact of different α , β , and γ values in Gated DA. Tab.6 shows the different impact of different value of (α , β , γ) in the proposed gatedDA. We noticed that when setting one of these parameters to 0, the performance is decreased. When we set (α , β , γ) to ($hidden/4$, $hidden/4$, $hidden/2$), the average performance is increased. This means each part of the proposed gatedDA is necessary. The visual features shown in Fig. 6 indicate that α , β , and γ consistently focus on various aspects of the degraded regions, each specializing in different levels or types of degradation.

5. Discussion

What does the proposed Skip-Split bring? Adjacent channels often contain redundant information due to spatial correlations in the data. Directly splitting the channels into two contiguous halves can lead to uneven feature distribution, with one half potentially capturing redundant features while the other lacks important information. By using a simple skip-split method that interleaves channels between the two processing paths, we ensure a more balanced and diverse set of features in each path, enhancing the effectiveness of both the self-attention and convolutional components. These phenomena is also validated in Fig. 7.

Why does the proposed GatedDA work? As shown in Fig. 8, the error map visualization reveals that degradation in an input image is often not evenly distributed, instead presenting as both global patterns and localized clusters. This suggests that effective degradation modeling must capture both widespread and specific distortions. The proposed GatedDA module addresses this need by targeting its feature responses specifically on degraded regions, achieving a close alignment with the error map. This focus underscores GatedDA’s capacity to selectively enhance degradation features, and when combined with global attention, it provides a comprehensive representation of the image’s degradation structure. This synergy between GatedDA and global attention improves overall restoration quality by allowing nu-

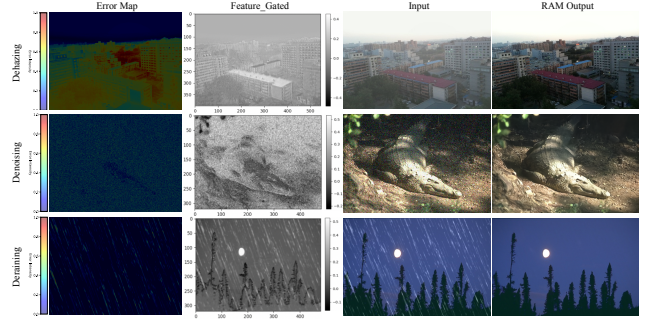


Figure 8. Visualization of the error map and the output of GatedDA.

anced handling of various degradation types. Importantly, our results demonstrate that GatedDA maintains this adaptability across diverse degradation conditions, emphasizing its robustness and versatility in restoration tasks.

Why is RAM efficient? RAM reduces computational costs by splitting input channels: one half is processed by self-attention, the other by a Gated CNN block. This division halves the self-attention’s complexity from $O(B \cdot head \cdot (H \cdot W)^2)$, while the Gated CNN processes the remaining channels with a lower complexity of $O(B \cdot C \cdot H \cdot W)$, especially beneficial for high-resolution inputs where $(H \cdot W)^2$ dominates. Additionally, RAM employs dimensionality reduction and parameter-efficient designs, collectively reducing GFLOPs and model parameters. This balance of global context modeling and efficient local feature extraction enables RAM to minimize computational costs without sacrificing performance.

Is scaling down the new advantage? While recent methods in image restoration often scale up model size and complexity, our approach takes a different path: scaling down. Instead of relying on large architectures, we embrace a simple but non-trivial design, using targeted components like the GatedDA module to effectively capture degradation without excessive parameters. This simplicity is not a compromise; it’s an asset—yielding high-quality restoration with minimal computational demand, faster training, and greater adaptability. The All-in-One IR framework, though new compared to degradation-specific methods, faces a key limitation: an imbalance in data distribution, with certain degradations (*e.g.*, dehazing) dominating. Our experiments suggest that a more balanced dataset could significantly improve performance across degradation types, offering a constructive direction for future work. Additional analyses, experiments, and visual results are available in our *Supp. Mat.*

6. Conclusion

We introduce RAM, an efficient single-image restoration model capable of handling any type of degradation. Our model leverages the intrinsic characteristics of each degradation as gated guidance, directing the overall feature modeling process. This approach enables the joint embedding of all

degradation types while preserving each of their unique attributes. RAM sets a new standard in degradation awareness, achieving unparalleled efficiency and fidelity in all-in-one image restoration. We hope that our model will serve as a fresh baseline for future research in this field.

References

- [1] Mark R Banham and Aggelos K Katsaggelos. Digital image restoration. *IEEE Signal Processing Magazine*, 14(2):24–41, 1997. 2
- [2] Dana Berman, Tali Treibitz, and Shai Avidan. Non-local image dehazing. In *CVPR*, pages 1674–1682, 2016. 1
- [3] Bolun Cai, Xiangmin Xu, Kui Jia, Chunmei Qing, and Dacheng Tao. Dehazenet: An end-to-end system for single image haze removal. *IEEE TIP*, 25(11):5187–5198, 2016. 1, 6
- [4] Jialun Cai, Weibo Huang, Yingxuan You, Zhan Chen, Bin Ren, and Hong Liu. Spasd: Semantics and deep reinforcement learning based motion planning for supermarket robot. *IEICE TRANSACTIONS on Information and Systems*, 106(5):765–772, 2023. 1
- [5] Liangyu Chen, Xiaojie Chu, Xiangyu Zhang, and Jian Sun. Simple baselines for image restoration. In *ECCV*, pages 17–33, 2022. 1, 5, 6
- [6] Xiangyu Chen, Xintao Wang, Jiantao Zhou, Yu Qiao, and Chao Dong. Activating more pixels in image super-resolution transformer. In *CVPR*, pages 22367–22377, 2023. 4
- [7] Yinbo Chen, Sifei Liu, and Xiaolong Wang. Learning continuous image representation with local implicit image function. In *CVPR*, pages 8628–8638, 2021. 2
- [8] Zheng Chen, Yulun Zhang, Jinjin Gu, Yongbing Zhang, Linghe Kong, and Xin Yuan. Cross aggregation transformer for image restoration. *NeurIPS*, 35:25478–25490, 2022. 1
- [9] Zheng Chen, Yulun Zhang, Jinjin Gu, Linghe Kong, and Xiaokang Yang. Recursive generalization transformer for image super-resolution. *arXiv preprint arXiv:2303.06373*, 2023. 4
- [10] Zheng Chen, Yulun Zhang, Jinjin Gu, Linghe Kong, Xiaokang Yang, and Fisher Yu. Dual aggregation transformer for image super-resolution. In *Proceedings of the IEEE/CVF International Conference on Computer Vision*, 2023. 4
- [11] Marcos V Conde, Gregor Geigle, and Radu Timofte. Instructir: High-quality image restoration following human instructions. In *Proceedings of the European Conference on Computer Vision (ECCV)*, 2024. 5, 6
- [12] Marcos V. Conde, Gregor Geigle, and Radu Timofte. Instructir: High-quality image restoration following human instructions. *arXiv preprint arXiv:2401.16468*, 2024. 2
- [13] Yuning Cui, Syed Waqas Zamir, Salman Khan, Alois Knoll, Mubarak Shah, and Fahad Shahbaz Khan. Adair: Adaptive all-in-one image restoration via frequency mining and modulation. *arXiv preprint arXiv:2403.14614*, 2024. 3
- [14] Kostadin Dabov, Alessandro Foi, Vladimir Katkovnik, and Karen Egiazarian. Color image denoising via sparse 3d collaborative filtering with grouping constraint in luminance-chrominance space. In *2007 IEEE international conference on image processing*, pages I–313. IEEE, 2007. 6
- [15] Tri Dao and Albert Gu. Transformers are SSMs: Generalized models and efficient algorithms through structured state space duality. In *International Conference on Machine Learning (ICML)*, 2024. 2, 3
- [16] Chao Dong, Yubin Deng, Chen Change Loy, and Xiaoou Tang. Compression artifacts reduction by a deep convolutional network. In *ICCV*, pages 576–584, 2015. 1, 2
- [17] Yu Dong, Yihao Liu, He Zhang, Shifeng Chen, and Yu Qiao. Fd-gan: Generative adversarial networks with fusion-discriminator for single image dehazing. In *Proceedings of the AAAI conference on artificial intelligence (AAAI)*, 2020. 5, 6
- [18] Alexey Dosovitskiy, Lucas Beyer, Alexander Kolesnikov, Dirk Weissenborn, Xiaohua Zhai, Thomas Unterthiner, Mostafa Dehghani, Matthias Minderer, Georg Heigold, Sylvain Gelly, et al. An image is worth 16x16 words: Transformers for image recognition at scale. In *ICLR*, 2020. 2, 4
- [19] Huiyu Duan, Xiongkuo Min, Sijing Wu, Wei Shen, and Guangtao Zhai. Uniprocessor: a text-induced unified low-level image processor. In *European Conference on Computer Vision*, pages 180–199. Springer, 2025. 5
- [20] Akshay Dudhane, Omkar Thawakar, Syed Waqas Zamir, Salman Khan, Fahad Shahbaz Khan, and Ming-Hsuan Yang. Dynamic pre-training: Towards efficient and scalable all-in-one image restoration. *arXiv preprint arXiv:2404.02154*, 2024. 3
- [21] Max Ehrlich, Larry Davis, Ser-Nam Lim, and Abhinav Shrivastava. Quantization guided JPEG artifact correction. In *ECCV*, pages 293–309, 2020. 1
- [22] Qingnan Fan, Dongdong Chen, Lu Yuan, Gang Hua, Nenghai Yu, and Baoquan Chen. A general decoupled learning framework for parameterized image operators. *IEEE transactions on pattern analysis and machine intelligence*, 43(1):33–47, 2019. 5, 6
- [23] Hongyun Gao, Xin Tao, Xiaoyong Shen, and Jiaya Jia. Dynamic scene deblurring with parameter selective sharing and nested skip connections. In *CVPR*, 2019. 5, 6
- [24] Sicheng Gao, Xuhui Liu, Bohan Zeng, Sheng Xu, Yanjing Li, Xiaoyan Luo, Jianzhuang Liu, Xiantong Zhen, and Baochang Zhang. Implicit diffusion models for continuous super-resolution. In *CVPR*, pages 10021–10030, 2023. 2
- [25] Albert Gu and Tri Dao. Mamba: Linear-time sequence modeling with selective state spaces. *arXiv preprint arXiv:2312.00752*, 2023. 2, 3
- [26] Hang Guo, Jinmin Li, Tao Dai, Zhihao Ouyang, Xudong Ren, and Shu-Tao Xia. Mambair: A simple baseline for image restoration with state-space model. In *ECCV*, 2024. 2, 3, 6
- [27] Dan Hendrycks and Kevin Gimpel. Gaussian error linear units (gelus). *arXiv preprint arXiv:1606.08415*, 2016. 4, 5
- [28] Jiayi Jiang, Kai Zhang, and Radu Timofte. Towards flexible blind JPEG artifacts removal. In *ICCV*, pages 4997–5006, 2021. 1
- [29] Kui Jiang, Zhongyuan Wang, Peng Yi, Chen Chen, Baojin Huang, Yimin Luo, Jiayi Ma, and Junjun Jiang. Multi-scale progressive fusion network for single image deraining. In *Proceedings of the IEEE/CVF conference on computer vision and pattern recognition*, pages 8346–8355, 2020. 2, 6

- [30] Yitong Jiang, Zhaoyang Zhang, Tianfan Xue, and Jinwei Gu. Autodir: Automatic all-in-one image restoration with latent diffusion. *arXiv preprint arXiv:2310.10123*, 2023. 2
- [31] Lingshun Kong, Jiangxin Dong, Jianjun Ge, Mingqiang Li, and Jinshan Pan. Efficient frequency domain-based transformers for high-quality image deblurring. In *Proceedings of the IEEE/CVF Conference on Computer Vision and Pattern Recognition*, pages 5886–5895, 2023. 1, 2
- [32] Wei-Sheng Lai, Jia-Bin Huang, Narendra Ahuja, and Ming-Hsuan Yang. Deep laplacian pyramid networks for fast and accurate super-resolution. In *CVPR*, pages 624–632, 2017. 2
- [33] Boyi Li, Xiulian Peng, Zhangyang Wang, Jizheng Xu, and Dan Feng. Aod-net: All-in-one dehazing network. In *Proceedings of the IEEE international conference on computer vision*, pages 4770–4778, 2017. 6
- [34] Boyun Li, Xiao Liu, Peng Hu, Zhongqin Wu, Jiancheng Lv, and Xi Peng. All-In-One Image Restoration for Unknown Corruption. In *Proceedings of the IEEE/CVF Conference on Computer Vision and Pattern Recognition (CVPR)*, 2022. 1, 5, 6
- [35] Boyun Li, Xiao Liu, Peng Hu, Zhongqin Wu, Jiancheng Lv, and Xi Peng. All-in-one image restoration for unknown corruption. In *Proceedings of the IEEE/CVF conference on computer vision and pattern recognition*, pages 17452–17462, 2022. 2
- [36] Runde Li, Jinshan Pan, Zechao Li, and Jinhui Tang. Single image dehazing via conditional generative adversarial network. In *CVPR*, pages 8202–8211, 2018. 1
- [37] Ruoteng Li, Loong-Fah Cheong, and Robby T Tan. Heavy rain image restoration: Integrating physics model and conditional adversarial learning. In *CVPR*, pages 1633–1642, 2019.
- [38] Yu Li, Robby T Tan, Xiaojie Guo, Jiangbo Lu, and Michael S Brown. Rain streak removal using layer priors. In *CVPR*, pages 2736–2744, 2016. 1
- [39] Yawei Li, Yuchen Fan, Xiaoyu Xiang, Denis Demandolx, Rakesh Ranjan, Radu Timofte, and Luc Van Gool. Efficient and explicit modelling of image hierarchies for image restoration. In *CVPR*, pages 18278–18289, 2023. 1, 2, 4
- [40] Yawei Li, Kai Zhang, Jingyun Liang, Jiezhong Cao, Ce Liu, Rui Gong, Yulun Zhang, Hao Tang, Yun Liu, Denis Demandolx, Rakesh Ranjan, Radu Timofte, and Luc Van Gool. LS-DIR: A large scale dataset for image restoration. In *CVPRW*, pages 1775–1787, 2023. 2
- [41] Zilong Li, Yiming Lei, Chenglong Ma, Junping Zhang, and Hongming Shan. Prompt-in-prompt learning for universal image restoration. *arXiv preprint arXiv:2312.05038*, 2023. 2, 3
- [42] Jingyun Liang, Jiezhong Cao, Guolei Sun, Kai Zhang, Luc Van Gool, and Radu Timofte. SwinIR: Image restoration using Swin transformer. In *ICCVW*, pages 1833–1844, 2021. 1, 2, 4, 6
- [43] Bee Lim, Sanghyun Son, Heewon Kim, Seungjun Nah, and Kyoung Mu Lee. Enhanced deep residual networks for single image super-resolution. In *CVPRW*, pages 1132–1140, 2017. 2
- [44] Chang Liu, Mengyi Zhao, Bin Ren, Mengyuan Liu, Nicu Sebe, et al. Spatio-temporal graph diffusion for text-driven human motion generation. In *BMVC*, pages 722–729, 2023. 2
- [45] Hong Liu, Bin Ren, Mengyuan Liu, and Runwei Ding. Grouped temporal enhancement module for human action recognition. In *2020 IEEE International Conference on Image Processing (ICIP)*, pages 1801–1805. IEEE, 2020. 1
- [46] Lin Liu, Lingxi Xie, Xiaopeng Zhang, Shanxin Yuan, Xiangyu Chen, Wengang Zhou, Houqiang Li, and Qi Tian. Tape: Task-agnostic prior embedding for image restoration. In *Proceedings of the European Conference on Computer Vision (ECCV)*, 2022. 1, 6
- [47] Zhuang Liu, Hanzi Mao, Chao-Yuan Wu, Christoph Feichtenhofer, Trevor Darrell, and Saining Xie. A convnet for the 2020s. In *Proceedings of the IEEE/CVF conference on computer vision and pattern recognition*, pages 11976–11986, 2022. 3
- [48] Ziwei Luo, Fredrik K Gustafsson, Zheng Zhao, Jens Sjölund, and Thomas B Schön. Image restoration with mean-reverting stochastic differential equations. *arXiv preprint arXiv:2301.11699*, 2023. 2
- [49] Ziwei Luo, Fredrik K Gustafsson, Zheng Zhao, Jens Sjölund, and Thomas B Schön. Controlling vision-language models for universal image restoration. In *ICLR*, 2024. 2, 5
- [50] Rafael Molina, Jorge Núñez, Francisco J Cortijo, and Javier Mateos. Image restoration in astronomy: a Bayesian perspective. *IEEE Signal Processing Magazine*, 18(2):11–29, 2001. 1
- [51] Chong Mou, Qian Wang, and Jian Zhang. Deep generalized unfolding networks for image restoration. In *Proceedings of the IEEE/CVF conference on computer vision and pattern recognition*, pages 17399–17410, 2022. 6
- [52] Jinshan Pan, Zhe Hu, Zhixun Su, and Ming-Hsuan Yang. Deblurring text images via l0-regularized intensity and gradient prior. In *CVPR*, pages 2901–2908, 2014. 1
- [53] Vaishnav Potlapalli, Syed Waqas Zamir, Salman H Khan, and Fahad Shahbaz Khan. Promptir: Prompting for all-in-one image restoration. *Advances in Neural Information Processing Systems*, 36, 2024. 1, 2, 3, 4, 5, 6
- [54] Yanyun Qu, Yizi Chen, Jingying Huang, and Yuan Xie. Enhanced pix2pix dehazing network. In *Proceedings of the IEEE/CVF conference on computer vision and pattern recognition*, pages 8160–8168, 2019. 6
- [55] Bin Ren, Yahui Liu, Yue Song, Wei Bi, Rita Cucchiara, Nicu Sebe, and Wei Wang. Masked jigsaw puzzle: A versatile position embedding for vision transformers. In *CVPR*, pages 20382–20391, 2023. 2
- [56] Bin Ren, Yawei Li, Nancy Mehta, Radu Timofte, Hongyuan Yu, Cheng Wan, Yuxin Hong, Bingnan Han, Zhuoyuan Wu, Yajun Zou, et al. The ninth nire 2024 efficient super-resolution challenge report. In *Proceedings of the IEEE/CVF Conference on Computer Vision and Pattern Recognition*, pages 6595–6631, 2024. 1
- [57] Dongwei Ren, Wangmeng Zuo, Qinghua Hu, Pengfei Zhu, and Deyu Meng. Progressive image deraining networks: A better and simpler baseline. In *Proceedings of the IEEE/CVF conference on computer vision and pattern recognition*, pages 3937–3946, 2019. 2

- [58] Mengwei Ren, Mauricio Delbracio, Hossein Talebi, Guido Gerig, and Peyman Milanfar. Multiscale structure guided diffusion for image deblurring. In *ICCV*, pages 10721–10733, 2023. 2
- [59] Wenqi Ren, Si Liu, Hua Zhang, Jinshan Pan, Xiaochun Cao, and Ming-Hsuan Yang. Single image dehazing via multi-scale convolutional neural networks. In *ECCV*, pages 154–169, 2016. 6
- [60] Wenqi Ren, Jinshan Pan, Hua Zhang, Xiaochun Cao, and Ming-Hsuan Yang. Single image dehazing via multi-scale convolutional neural networks with holistic edges. *International Journal of Computer Vision*, 128:240–259, 2020. 2
- [61] William Hadley Richardson. Bayesian-based iterative method of image restoration. *Journal of the Optical Society of America*, 62(1):55–59, 1972. 2
- [62] Olaf Ronneberger, Philipp Fischer, and Thomas Brox. U-Net: Convolutional networks for biomedical image segmentation. In *Proceedings of International Conference on Medical Image Computing and Computer-Assisted Intervention*, pages 234–241, 2015. 3
- [63] MI Sezan and Henry Stark. Image restoration by the method of convex projections: Part 2-applications and numerical results. *IEEE TMI*, 1(2):95–101, 1982. 1
- [64] Qi Shan, Jiaya Jia, and Aseem Agarwala. High-quality motion deblurring from a single image. *ACM Transactions on Graphics (TOG)*, 27(3):1–10, 2008. 1
- [65] Chunwei Tian, Yong Xu, and Wangmeng Zuo. Image denoising using deep cnn with batch renormalization. *Neural Networks*, 2020. 5, 6
- [66] Chunwei Tian, Yong Xu, and Wangmeng Zuo. Image denoising using deep cnn with batch renormalization. *Neural Networks*, 121:461–473, 2020. 5
- [67] Fu-Jen Tsai, Yan-Tsung Peng, Chung-Chi Tsai, Yen-Yu Lin, and Chia-Wen Lin. BANet: A blur-aware attention network for dynamic scene deblurring. *IEEE TIP*, 31:6789–6799, 2022. 1
- [68] Zhengzhong Tu, Hossein Talebi, Han Zhang, Feng Yang, Peyman Milanfar, Alan Bovik, and Yinxiao Li. MAXIM: Multi-axis mlp for image processing. In *CVPR*, pages 5769–5780, 2022. 2
- [69] Jeya Maria Jose Valanarasu, Rajeev Yasarla, and Vishal M Patel. TransWeather: Transformer-based restoration of images degraded by adverse weather conditions. In *CVPR*, pages 2353–2363, 2022. 6
- [70] Cong Wang, Jinshan Pan, Wei Wang, Jiangxin Dong, Mengzhu Wang, Yakun Ju, and Junyang Chen. Promptrestorer: A prompting image restoration method with degradation perception. *Advances in Neural Information Processing Systems*, 36:8898–8912, 2023. 2, 3
- [71] Xintao Wang, Ke Yu, Chao Dong, and Chen Change Loy. Recovering realistic texture in image super-resolution by deep spatial feature transform. In *CVPR*, pages 606–615, 2018. 2
- [72] Yinhuai Wang, Jiwen Yu, and Jian Zhang. Zero-shot image restoration using denoising diffusion null-space model. *ICLR*, 2023. 2
- [73] Zhendong Wang, Xiaodong Cun, Jianmin Bao, Wengang Zhou, Jianzhuang Liu, and Houqiang Li. Uformer: A general u-shaped transformer for image restoration. In *CVPR*, pages 17683–17693, 2022. 1
- [74] Wei Wei, Deyu Meng, Qian Zhao, Zongben Xu, and Ying Wu. Semi-supervised transfer learning for image rain removal. In *Proceedings of the IEEE/CVF conference on computer vision and pattern recognition*, pages 3877–3886, 2019. 6
- [75] Gang Wu, Junjun Jiang, Kui Jiang, and Xianming Liu. Harmony in diversity: Improving all-in-one image restoration via multi-task collaboration. In *Proceedings of the 32nd ACM International Conference on Multimedia*, pages 6015–6023, 2024. 5
- [76] Haiyan Wu, Yanyun Qu, Shaohui Lin, Jian Zhou, Ruizhi Qiao, Zhizhong Zhang, Yuan Xie, and Lizhuang Ma. Contrastive learning for compact single image dehazing. In *Proceedings of the IEEE/CVF conference on computer vision and pattern recognition*, pages 10551–10560, 2021. 2
- [77] Wenhan Yang, Robby T Tan, Jiashi Feng, Jiaying Liu, Zongming Guo, and Shuicheng Yan. Deep joint rain detection and removal from a single image. In *CVPR*, pages 1357–1366, 2017. 1
- [78] Rajeev Yasarla and Vishal M Patel. Uncertainty guided multi-scale residual learning-using a cycle spinning cnn for single image de-raining. In *Proceedings of the IEEE/CVF conference on computer vision and pattern recognition*, pages 8405–8414, 2019. 6
- [79] Weihao Yu, Mi Luo, Pan Zhou, Chenyang Si, Yichen Zhou, Xinchao Wang, Jiashi Feng, and Shuicheng Yan. Metaformer is actually what you need for vision. In *Proceedings of the IEEE/CVF conference on computer vision and pattern recognition*, pages 10819–10829, 2022. 3
- [80] Weihao Yu, Pan Zhou, Shuicheng Yan, and Xinchao Wang. Inceptionnext: When inception meets convnext. In *Proceedings of the IEEE/CVF Conference on Computer Vision and Pattern Recognition*, pages 5672–5683, 2024. 3
- [81] Zongsheng Yue, Jianyi Wang, and Chen Change Loy. ResShift: Efficient diffusion model for image super-resolution by residual shifting. *arXiv preprint arXiv:2307.12348*, 2023. 2
- [82] Eduard Zamfir, Zongwei Wu, Nancy Mehta, Danda Dani Paudel, Yulun Zhang, and Radu Timofte. Efficient degradation-aware any image restoration. *arXiv preprint arXiv:2405.15475*, 2024. 1, 3
- [83] Eduard Zamfir, Zongwei Wu, Nancy Mehta, Yulun Zhang, and Radu Timofte. See more details: Efficient image super-resolution by experts mining. In *International Conference on Machine Learning*. PMLR, 2024. 2
- [84] Syed Waqas Zamir, Aditya Arora, Salman Khan, Munawar Hayat, Fahad Shahbaz Khan, Ming-Hsuan Yang, and Ling Shao. Multi-stage progressive image restoration. In *CVPR*, pages 14821–14831, 2021. 1
- [85] Syed Waqas Zamir, Aditya Arora, Salman Khan, Munawar Hayat, Fahad Shahbaz Khan, Ming-Hsuan Yang, and Ling Shao. Multi-stage progressive image restoration. In *Proceedings of the IEEE/CVF Conference on Computer Vision and Pattern Recognition (CVPR)*, 2021. 5
- [86] Syed Waqas Zamir, Aditya Arora, Salman Khan, Munawar Hayat, Fahad Shahbaz Khan, and Ming-Hsuan Yang.

- Restormer: Efficient transformer for high-resolution image restoration. In *CVPR*, pages 5728–5739, 2022. [1](#), [2](#), [4](#), [5](#), [6](#)
- [87] He Zhang and Vishal M Patel. Density-aware single image de-raining using a multi-stream dense network. In *Proceedings of the IEEE conference on computer vision and pattern recognition*, pages 695–704, 2018. [6](#)
- [88] Jinghao Zhang, Jie Huang, Mingde Yao, Zizheng Yang, Hu Yu, Man Zhou, and Feng Zhao. Ingredient-oriented multi-degradation learning for image restoration. In *Proceedings of the IEEE/CVF Conference on Computer Vision and Pattern Recognition*, pages 5825–5835, 2023. [1](#), [2](#), [5](#), [6](#)
- [89] Kai Zhang, Wangmeng Zuo, Yunjin Chen, Deyu Meng, and Lei Zhang. Beyond a gaussian denoiser: Residual learning of deep cnn for image denoising. *IEEE TIP*, 26(7):3142–3155, 2017. [1](#), [2](#), [6](#)
- [90] Kai Zhang, Wangmeng Zuo, Shuhang Gu, and Lei Zhang. Learning deep cnn denoiser prior for image restoration. In *CVPR*, pages 3929–3938, 2017. [2](#), [6](#)
- [91] Kai Zhang, Wangmeng Zuo, and Lei Zhang. FFDNet: Toward a fast and flexible solution for cnn-based image denoising. *IEEE TIP*, 27(9):4608–4622, 2018. [1](#), [6](#)
- [92] Leheng Zhang, Yawei Li, Xingyu Zhou, Xiaorui Zhao, and Shuhang Gu. Transcending the limit of local window: Advanced super-resolution transformer with adaptive token dictionary. *arXiv preprint arXiv:2401.08209*, 2024. [2](#)
- [93] Xu Zhang, Jiaqi Ma, Guoli Wang, Qian Zhang, Huan Zhang, and Lefei Zhang. Perceive-ir: Learning to perceive degradation better for all-in-one image restoration. *arXiv preprint arXiv:2408.15994*, 2024. [6](#)
- [94] Yulun Zhang, Kunpeng Li, Kai Li, Bineng Zhong, and Yun Fu. Residual non-local attention networks for image restoration. *arXiv preprint arXiv:1903.10082*, 2019. [2](#)
- [95] Mengyi Zhao, Mengyuan Liu, Bin Ren, Shuling Dai, and Nicu Sebe. Denoising diffusion probabilistic models for action-conditioned 3d motion generation. In *ICASSP 2024-2024 IEEE International Conference on Acoustics, Speech and Signal Processing (ICASSP)*, pages 4225–4229. IEEE, 2024. [2](#)
- [96] Lianghui Zhu, Bencheng Liao, Qian Zhang, Xinlong Wang, Wenyu Liu, and Xinggang Wang. Vision mamba: Efficient visual representation learning with bidirectional state space model. *arXiv preprint arXiv:2401.09417*, 2024. [2](#)